Journal of Materials Chemistry C

Accepted Manuscript

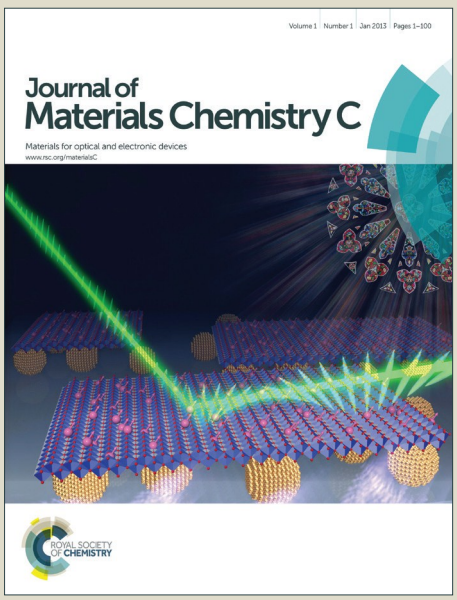

ROYAL SOCIETY OF CHEMISTRY

www.rsc.org/materialsC

Novel Blue and Green Phosphors Yielded in $K_2ZrSi_3O_9$: Eu^{2+} Compound by Different Charge Compensation Ions for LEDs under Near-UV Excitation

Xin Ding[ab], Ge Zhu[ab], Wanying Geng[ab], ‡Masayoshi Mikami[c], Yuhua Wang[ab]*

[a]*Department of Materials Science, School of Physical Science and Technology, Lanzhou University*

[b]*Key Laborary of Special Function Materials and Structure Design, Ministry of Education, Lanzhou University, Tianshui South Road No. 222, Lanzhou, Gansu 730000, PR China*

[c]*Mitsubishi Chemical Group Science and Technology Research Center,Inc.,1000 Kamoshida-cho,Aoba-ku, Yokohama 227-8502, Japan*

Abstract

The structural properties of wadeite $K_2ZrSi_3O_9$ have been investigated using the high-resolution transmission electron microscopy and X-ray powder diffraction refinement, and the luminescence properties of Eu^{2+} activated $K_2ZrSi_3O_9$ have been studied to explore the new materials for phosphor-converted white light near ultraviolet light-emitting diodes (NUV-LEDs). Eu^{2+} was introduced into the $K_2ZrSi_3O_9$ host in the reducing atmosphere, and the special crystallographic positions of the Eu^{2+} were determined based on XRD, photoluminescence emission spectra, temperature dependence properties, time-resolved photoluminescence etc..The calculated band gap is about 4.7 eV. The CIE chromaticity coordinates and FWHM of the blue phosphor $K_2ZrSi_3O_9$: 1%Eu^{2+} are (0.1538, 0.1857) and 57 nm. The photoluminescence properties of co-doped Eu^{2+}-$Al^{3+}$and Eu^{2+}-Sc^{3+} charge compensation pairs phosphors were investigated. The Eu^{2+} single-doped $K_2ZrSi_3O_9$ phosphor shows blue emission with the broad-band peaking at 465 nm upon 400 nm NUV excitation. By Eu^{2+}-Al^{3+} as charge compensation, the photoluminescence properties do not change distinctly, while the photoluminescence emission spectrum shifts to red area about 39 nm and becomes green emission by using Eu^{2+}-Sc^{3+} pair. Different occupying situations with different charge compensation pairs were discussed. Blue and green emission can be yielded in $K_2ZrSi_3O_9$: Eu^{2+} compound by different charge compensation mechanism. It reveals that $K_2ZrSi_3O_9$: Eu^{2+} possesses remarkable optical properties and can be used in NUV-LEDs.

Keywords: Phosphor, Photoluminescence, LED

*Corresponding author at: Department of Materials Science, School of Physical Science and Technology, Lanzhou University, Lanzhou, 730000, PR China.

Tel.: +86 931 8912772; fax: +86 931 8913554.

Corresponding author' email: wyh@lzu.edu.cn

‡MCHC R&D Synergy Center, Inc., 1000 Kamoshida-cho, Aoba-ku, Yokohama, Kanagawa 227-8502, Japan

1. Introduction

Nowadays, white light emitting diodes (W-LEDs) have attracted considerable attention and been used in many areas [1, 2] for their various advantages such as small volume, high efficiency, long lifetime, energy saving and environment-friendly [3]. The initial method to get W-LED lamp is consisting of three triple LED chips for red, green and blue [4]. Though it is easy to fabricate, it has different thermal stability, drive voltage, degradation and expensive for different LED chips [5-7], which restrains its application. Another feasible scheme for W-LED generation is using blue or ultraviolet chips combining with some phosphors which can be excited by them. For instance, YAG: Ce^{3+} yellow phosphor excited by blue InGaN chips can generate white light by mixing yellow emission from the phosphor and blue light from the chip. Though it has been to be commercialized and widely used, it cannot satisfy the optimum requirements. Different

degradation for blue chip and phosphor leads to chromatic aberration. Lack of red light component causes high correlated color temperature (7765K) and poor color rendering index which restricts its more broad applications [8-10]. In addition to this method, another kind of W-LEDs can be fabricated by combing of the GaN-based blue chip with green and red phosphors or via coupling ultraviolet (UV) LED (350–420 nm) with blue, green and red phosphors [11-14]. As compared to YAG: Ce^{3+} yellow phosphor excited by a blue InGaN chip, this type of W-LEDs has low correlated color temperature and high color rendering index (Ra > 90) [15]. There have been many reports describing the development of the tri-color emission phosphors for n-UV LED chips, and green or blue-emitting phosphors possess a large proportion in it. Some nitrides/oxynitrides green phosphors like $MSi_2O_2N_2$:Eu^{2+} and SiAlON: Eu^{2+} have been commercial [16, 17]. However, a well-known defect is that the synthesis of nitride phosphors needs a critical condition, such as high temperature and high pressure. In addition, many Eu^{2+} and Ce^{3+} doped oxide-based green or blue phosphors have been found, like $Ca_3Sc_2Si_3O_{12}$: Ce^{3+}, Ba_2SiO_4: Eu^{2+}, $Cs_{2x}Ca_{2x}Gd_{2(1-x)}(PO_4)_2$: Eu^{2+} and $BaMgAl_{10}O_{17}$: Eu^{2+} [18-21]. Yet, there are a few compounds doping with one kind rare earths ion which emit different light except some solid-solution phosphors [22-26].

The structure of $K_2ZrSi_3O_9$ (wadeite) crystal belongs to hexagonal (space group P63/m) consisting of planar three-membered silicate rings (Si_3O_9) linked by K^+ and Zr^{4+} ions. There are two symmetrically distinct oxygens: O(1) is bonded to two Si and two K atoms, and O(2) is bonded to one Si, one Zr, and two K atoms. There is only one lattice site for K, Zr and Si, respectively [27, 28]. The structure photoluminescence properties of wadeite $K_2ZrSi_3O_9$ doped with Eu^{2+} phosphors were first studied in this work. By co-doping different ions and adjusting the occupying sites of Eu^{2+}, blue and green light can yield in $K_2ZrSi_3O_9$: Eu^{2+} compound.

2. Experimental Section

2.1 Materials and utensil

K_2CO_3 (99.9%), ZrO_2 (99.99%), H_2SiO_3 (AR), $Al(OH)_3$ (AR), Sc_2O_3 (99.99%) and Eu_2O_3 (99.99%) as the raw materials are stoichiometric and 2.5wt% carbon powder as one of the reductant is also used in the synthesis process. Aluminum oxide crucibles (10 mm*10 mm) and porcelain boat are utensils for sintering.

2.2 Synthesis

A series of $K_2ZrSi_3O_9$: Eu^{2+} ($0.1 \leq x \leq 9\%$) samples are synthesized by two-step traditional high temperature solid-sated reaction. The relative amounts of materials are calculated and then are weighed by electronic balance accurate to 4 decimal places. Put all the raw materials and carbon powder into agate mortar with 8 mL ethanol added in it at the same time. Grind the mixture for 30 min until they are evenly blended and homogeneous. After the mixture dry, transfer the mixture into aluminum oxide crucibles (10 mm*10 mm) and pre-fire at 800 °C for 2 h under air atmosphere, then, calcine them at 1380 °C for 6 h under flowing 95% N_2−5% H_2 atmosphere in the horizontal tube furnace. When they are cooled with 5 °C /min speed to room temperature, grind them to powders, yielding the resulting phosphor powder.

2.3 Characterization

HRTEM (High-resolution transmission electron microscopy) is carried out on a transmission electron microscope at an operating voltage of 200 kV. The phase formation and crystal structure were analyzed by the X-ray powder diffraction (XRD) (D2 PHASER X-ray Diffractometer ,Germany) with graphite monochromator using Cu Kα radiation（λ = 1.54056 A), operating at 30 kV and 15 mA. The investigation range is 10 ^{o} to 80 ^{o} with scanning speed of 15 ^{o}

2θ min^{-1} for the series $K_{2-x}Eu_xZrSi_3O_9$ ($0.002 \leq x \leq 0.18$) samples and 10 °-90 ° with 2 ° 2θ min^{-1} for the structural refinement data. The photoluminescence (PL) and photoluminescence excitation (PLE) spectra of the samples are measured by a Fluorlog-3 spectrofluorometer equipped with 450 W xenon lamps (Horiba Jobin Yvon). The temperature-dependence luminescence properties are measured on the same spectrophotometer, which is combined with a self-made heating attachment and a computer-controlled electric furnace from room temperature (25 °C) to 250 °C with a heating rate of 100 °C/min and a holding time of 5 min for each temperature point. The luminescence decay curves and Time-resolved photoluminescence (TRPL) were obtained by FLS-920T fluorescence spectrophotometer as well. All the testes are carried out at room temperature. Raman spectra are measured by LabRam-80 (λ = 532 nm, Horiba Jobin Yvon, Japan)

3. Results and Discussion

3.1 Composition and Structural Characteristics of $K_2ZrSi_3O_9$

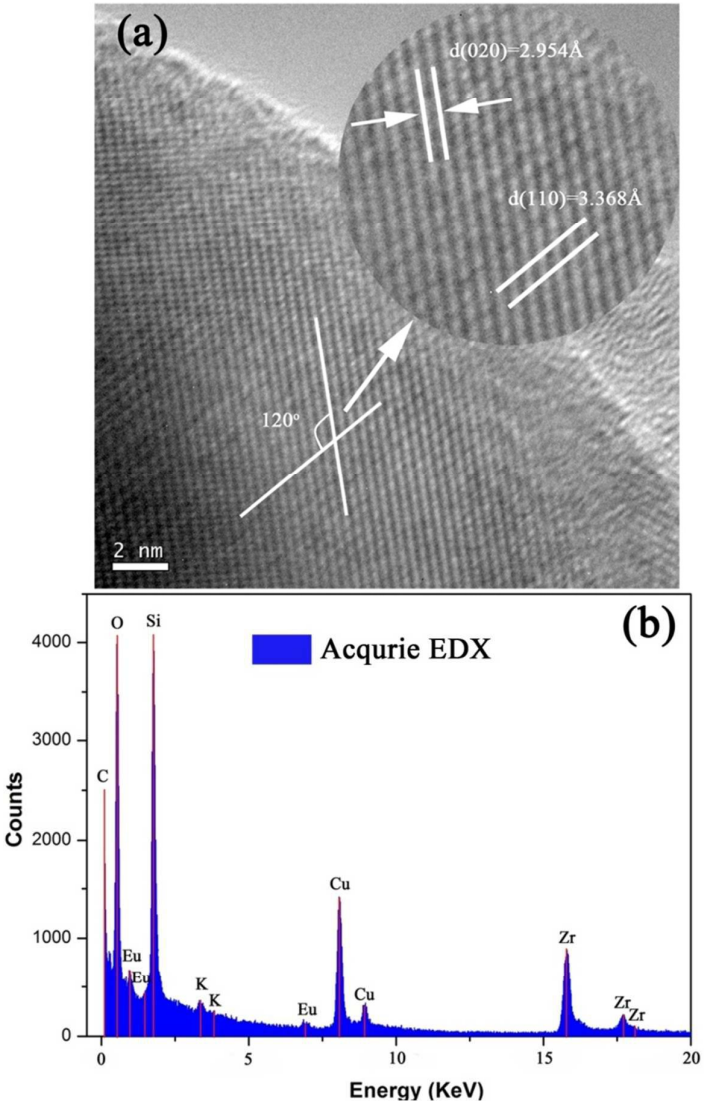

Figure 1: (a) HRTEM image of KZS: 1%Eu^{2+}; (b) EDX (energy-disperse x-ray analysis)

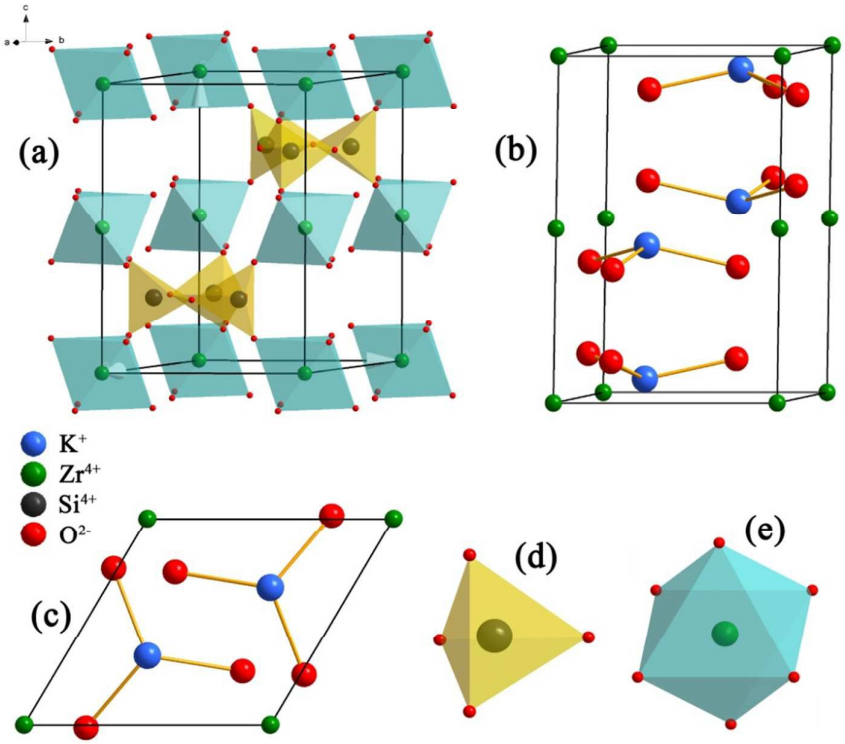

Figure 2 The structure of $K_2ZrSi_3O_9$ and coordination environment of K^+, Si^{4+}, Zr^{4+}

The structure and composition of the $K_2ZrSi_3O_9$: 1%Eu^{2+} are well examined by HRTEM, EDX. In Figure 1a, there are two apparent interplanars belong to (020) and (110) according to calculation and measurement, which the angle between these two interplanars is 120°. The HRTEM image reveals that $K_2ZrSi_3O_9$ takes on characteristic preferred orientation yielding by solid-state reaction which can be certificated with two relative strong peaks in XRD patterns (shown in Figure 6). The structure of $K_2ZrSi_3O_9$ (wadeite) crystal is hexagonal (space group P63/m) consist of planar three-membered silicate rings (Si_3O_9) linked by K^+ and Zr^{4+} ions. The wadeite structure contains [Si_3O_9] rings that are connected by [ZrO_6] octahedra. K^+ ions are contained between the staggered Si_3O_9 rings. The structure consists of layers of [Si_3O_9] rings parallel to the (001) plane, linked by octahedrally coordinated Zr atoms into a three-dimensional framework which are shown in Figure 2. K atoms occupy the nine-coordinated cage sites that are staggered between neighboring layers of [Si_3O_9] rings. There are two symmetrically distinct oxygens: O(1) is bonded to two Si and two K atoms, and O(2) is bonded to one Si, one Zr, and two K atoms. There is only one lattice site for K, Zr and Si, respectively [27-29]. The chemical composition of this compound is further determined by EDX as shown in Figure. 1c. The signals of potassium (K), zirconium (Zr), oxygen (O), silicon (Si) and europium (Eu) suggest the presence of the corresponding element in the product (the carbon and Cu signal are due to the instrument).

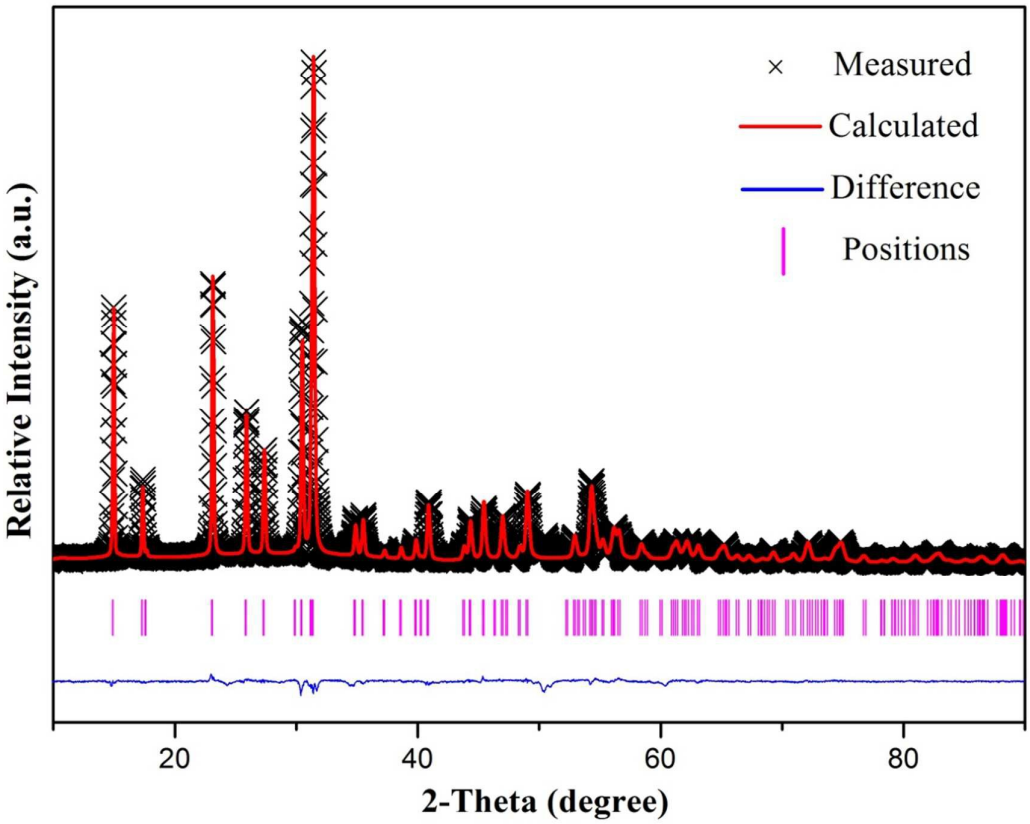

Figure 3 Rietveld refinement of the powder XRD profile of KZS: 1%Eu^{2+}

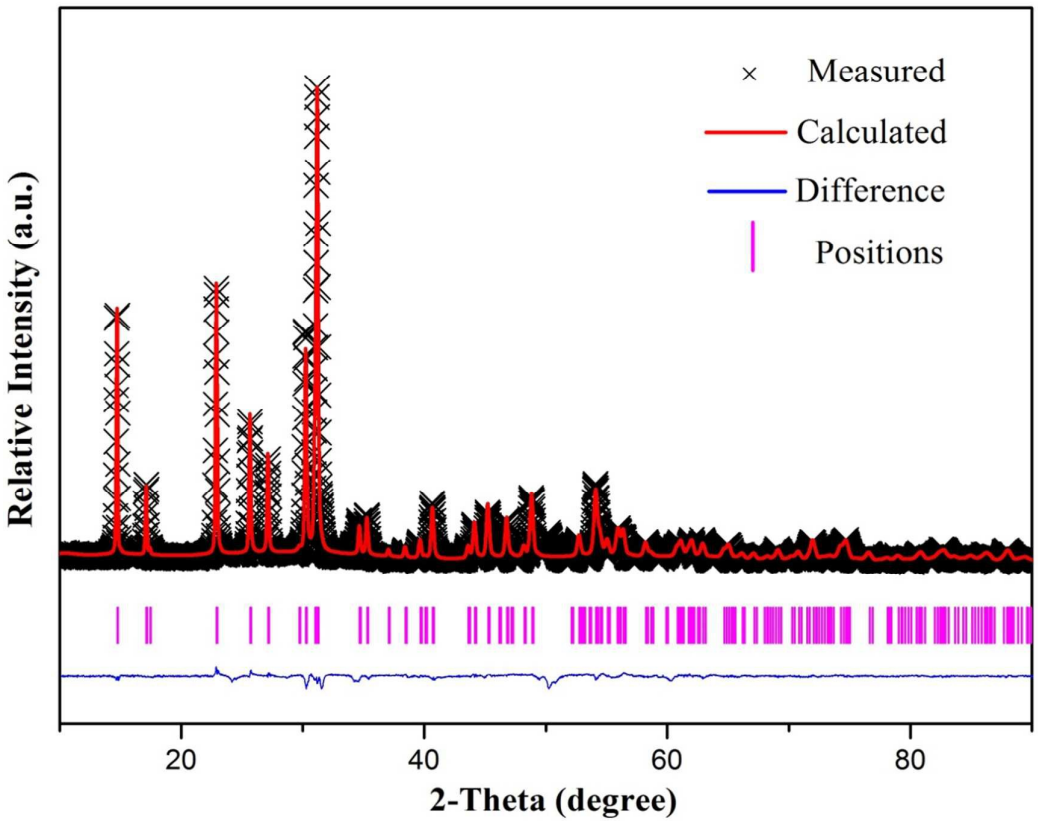

Figure 4 Rietveld refinement of the powder XRD profile of KZS: 1%Eu^{2+}, 1%Al^{3+}

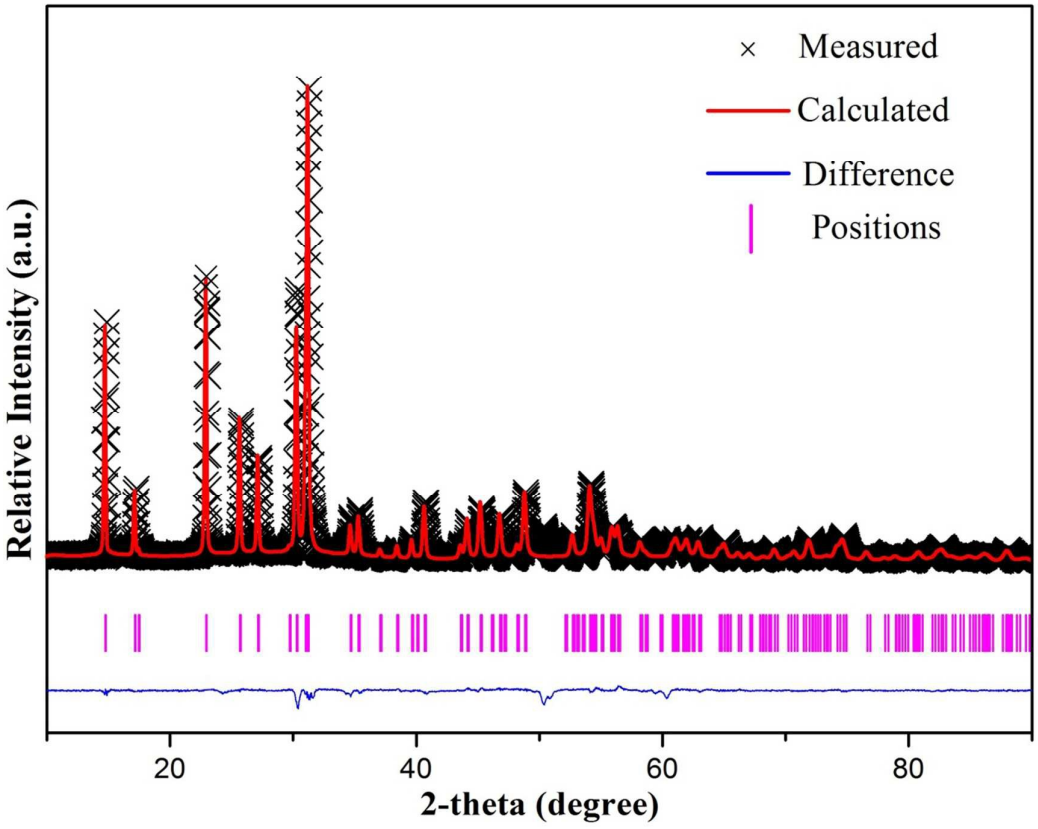

Figure 5 Rietveld refinement of the powder XRD profile of KZS: 1%Eu^{2+}, 1%Sc^{3+}

In order to determine the real structure of the synthesized samples, ICSD-171577 ($K_2ZrSi_3O_9$) was used as the standard data to refine KZS: 1%Eu^{2+}, KZS: 1%Eu^{2+}, 1%Al^{3+} and KZS: 1%Eu^{2+}, 1%Sc^{3+} samples and structural refinement of XRD was made using Materails Studio program. Figure 2, 3 and 4 illustrate the experimental and refined XRD patterns of these three samples. The "×" marks represent the measured diffraction data. The red solid curves indicate the calculated diffraction data and the pink vertical lines show the positions of the simulated diffraction patterns. The blue solid line denotes the deviation between the measured and calculated values. By comparing the calculated data with experimental spectra, we found that each peak is in good agreement. There is no impurity phase in the samples, which reveals that it is good single-phase. The calculated residual factor value is Rp = 6.15%, and Rwp = 7.83% for KZS: 1%Eu^{2+}; Rp = 7.48%, and Rwp = 9.26% for KZS: 1%Eu^{2+}, 1%Al^{3+}; Rp = 7.64%, and Rwp = 8.95% for KZS: 1%Eu^{2+}, 1%Sc^{3+}.

3.2 XRD Analysis of series KZS: x%Eu^{2+}

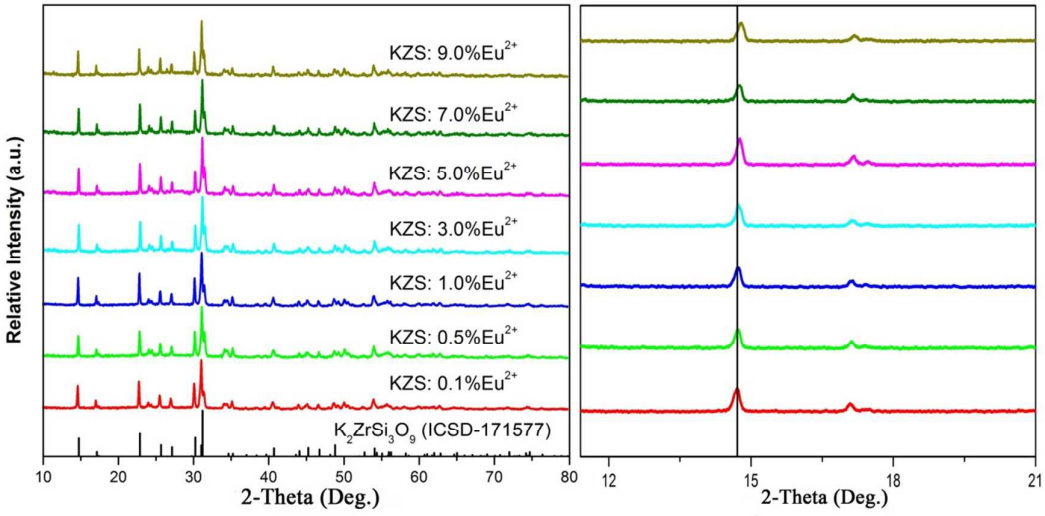

Figure 6 XRD patterns of series KZS: $x$$Eu^{2+}$ and calculated data (right image); Peak shift of series XRD patterns (left image).

XRD patterns of the as-prepared KZS: x%Eu^{2+} (x = 0.1, 0.5 1, 3, 5, 7, 9) phosphors were collected to verify the phase purity. As is given in Figure 6 right image, it can be seen that all of the diffraction peaks of the samples can be basically indexed to the corresponding standard data (Rietveld refinement data) except little excess peak around at 24 degree and suggesting that $K_2ZrSi_3O_9$: $x$$Eu^{2+}$ with different K/Eu ratios can be formed in the practical single-phased structure. In the meantime, the diffraction peaks shift to higher angles with increasing Eu^{2+} content (shown in left image) owing to the different ionic radius between K^+ (1.37 Å) and Eu^{2+} (1.17 Å). This shift can be explained by bragg equation ($2d\sin\phi = n\lambda$), If Eu^{2+} substitutes K^+, the interplanar spacing (d) becomes short, due to smaller radius of Eu^{2+} (1.17 Å) than K^+ (1.37 Å). The changes of the interplanar spacing (d) can be also observed in the HRTEM image shown in Figure 1a. In the no-doped $K_2ZrSi_3O_9$ host, the size of (020) and (110) two interplanars are 3.0034 Å and 3.4680 Å [28], larger than Eu^{2+}-doped sample. It indicated that Eu^{2+} have been doped into the crystal lattices of the hexagonal $K_2ZrSi_3O_9$ instead of forming the impurity phase.

3.3 The diffuse reflectance spectra of KZS: xEu^{2+}

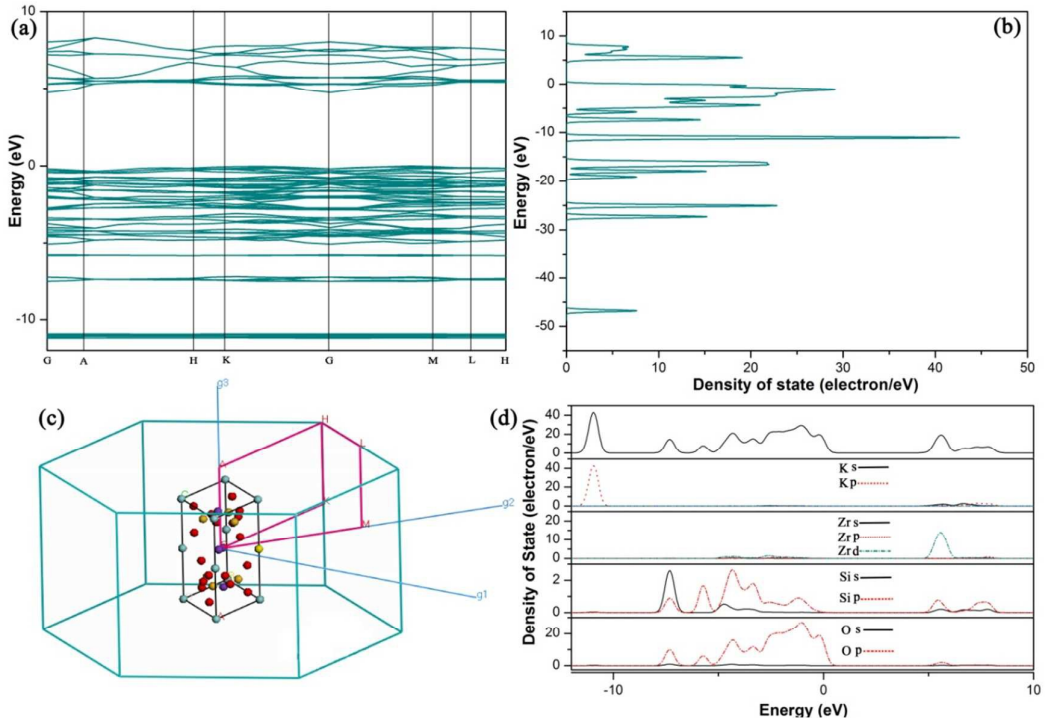

Figure 7 (a) Band structure of KZS; (b) Density of state; (c) Brillouin zone, (d) Total and partial density of states in the range from -12 to 10 eV.

The density functional theory calculations of KZS based on crystal structure data are shown in Fig. 7. The local density approximation (LDA) was chosen as the theoretical basis of the density function. This compound possesses an indirect band gap of about 4.7 eV with the valence band (VB) maximum at the K point and the conduction band (CB) minimum at the G point of the Brillouin zone. It is expected that the value of the calculated band gap of about 4.7 eV is smaller than the experimental one as the LDA underestimates the size of the band gap in general. The VB originates predominantly from K 3p, O 2p states, whereas the CB is composed mostly of K 4s, Si 3p and Zr 4d states. With such a large band gap, it is expected that the energy levels of the $4f^6 5d \leftrightarrow 4f^7$ transitions of the Eu^{2+} ion in the host lattice of KZS should have small interferences with the valence and conduction bands and the KZS host may provide a suitable band gap for Eu^{2+} to act as an emission center [30, 31].

3.4 Luminescence Properties of KZS: x%Eu^{2+}

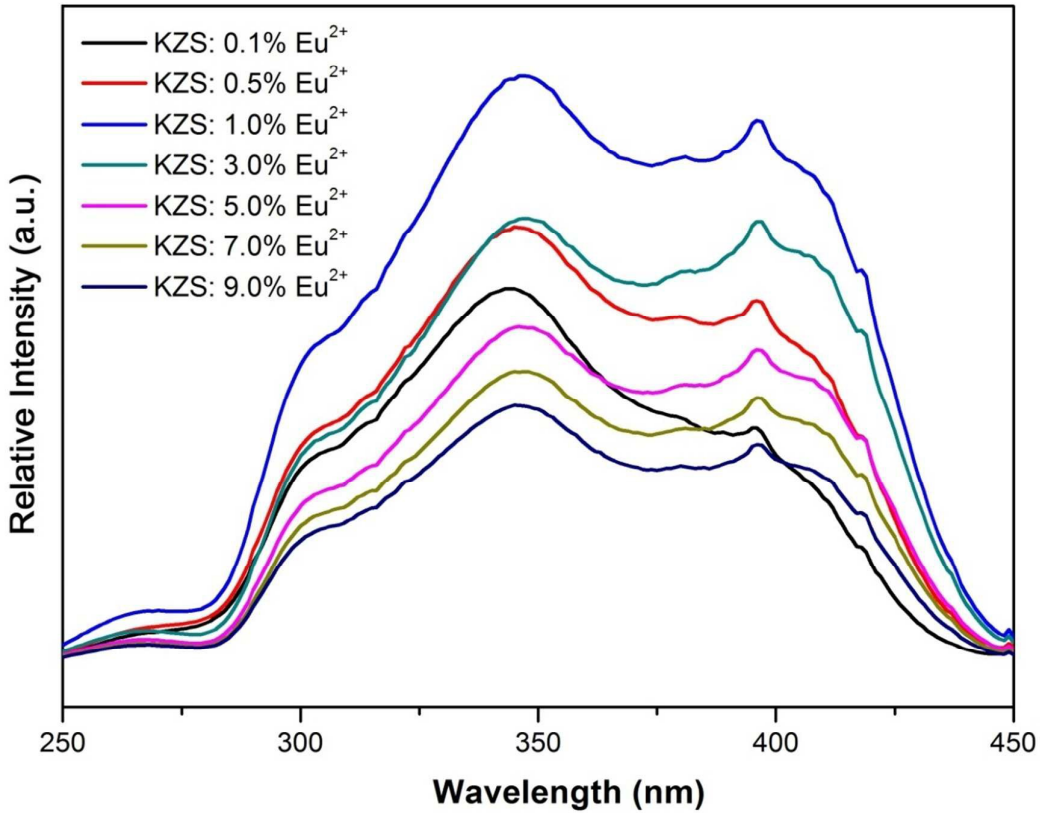

Figure 8 PLE properties with 1 nm slit of series KZS: x%Eu^{2+} phosphors

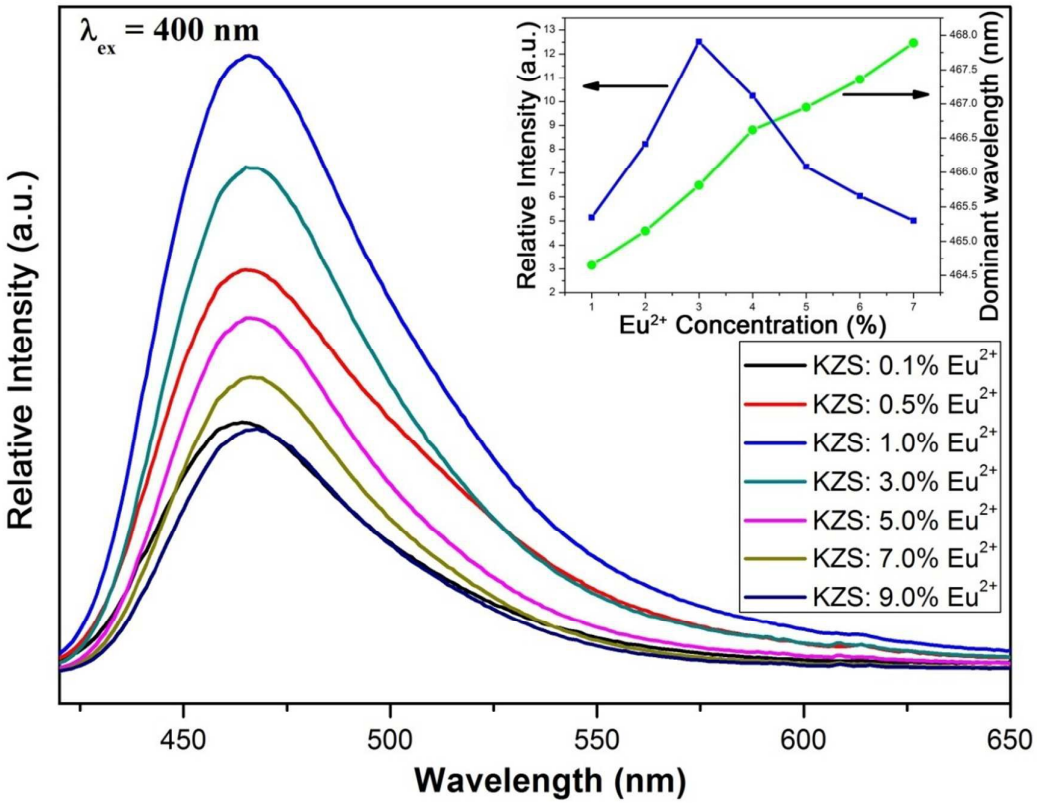

Figure 9 PL properties under 400 nm excitation with 1 nm slit of series KZS: x%Eu^{2+} phosphors; Inset: (Upper right) Dependence of emission intensity and peak position of KZS: x%Eu^{2+} phosphors on Ce^{3+} content

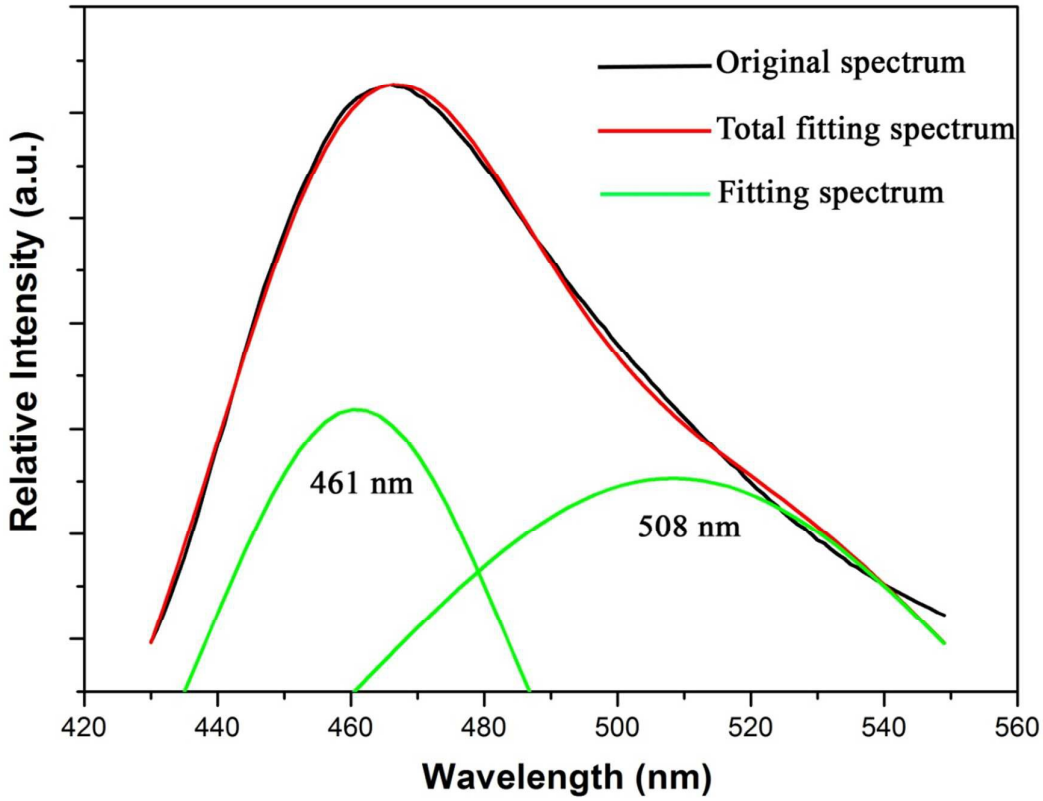

Figure 10 Gaussian components fitted of PL spectra

The PLE and PL spectra properties of series of KZS: x%Eu^{2+} depending on the x value are shown in Figure 8 and 9. The results illustrate that all of the PLE spectra of the materials show characteristic excitation bands of Eu^{2+} ions, which are broadly in the range from 300 nm to 450 nm. That can match NUV chips very well. Furthermore, the PLE spectra consist of four distinct bands originating from the f-d transition of Eu^{2+}. With the excitation of 400 nm, all the samples can emit blue light around 465 nm, which are attributed to the $4f^6 5d–4f^7$ transition of the Eu^{2+} [32]. Furthermore, it has little Eu^{3+} PLE and PL peak around 396 and 616 nm, but it does not affect the whole spectra obviously. In addition, from the inset of Figure 9, it can be easily seen that the emission intensities have an obvious increasing trend with increasing Eu^{2+} concentration, and maximizes at x = 0.01, then the emission intensity decreases attributed to concentration quenching. The peak position has apparent red shift from 465 to 468 nm about 138 cm^{-1}. With the increasing of Eu^{2+} content, the energy transfer of intra-Eu^{2+} becomes to be significant, this kind energy transfer that also leads to red shift of emission spectra. Besides, in KZS host, the relative smaller dopant Eu^{2+} occupies K^+ site will lead to red shift of emission spectra [33].

$$D_q = \frac{1}{6} Ze^2 \frac{r^4}{R^5} \quad (1)$$

Where Dq is a measure of the energy level separation, Z is the anion charge, e is the electron charge, r is the radius of the d wave function, and R is the bond length. When the K^+ ion is substituted and occupied by a smaller Eu^{2+} ion, the distance between the Eu^{2+} and O^{2-} ion becomes shorter. Since crystal field splitting is proportional to $1/R^5$, this shorter Eu^{2+}–O^{2-}distance also leads to the enhancement of crystal field strength surrounding the Eu^{2+} ion and further results in a larger crystal field splitting of Eu^{2+} 5*d* energy levels, which makes the lowest 5*d* state of Eu^{2+} closer to

its ground state and finally gives a red shift of the PL emission peak of the Eu^{2+}.

Furthermore, there is an interesting phenomenon that the emission bands are abnormal asymmetric, which are conflicting with only single K^+ site in $K_2ZrSi_3O_9$ lattice. The broad band can be fitted by two peaks at 461 and 508 nm using gaussian components. A possible reason is that Eu^{2+} occupies not only K^+ but also Zr^{4+} site which is shown in Figure 15(a). In the $K_2ZrSi_3O_9$ host, the radius of Eu^{2+} is 1.17 Å, smaller than K^+ (1.37 Å) and larger than Zr^{4+} (0.86 Å) but more close to K^+ [34]. Therefore, most of the dopant Eu^{2+} substitute K^+ and minority replace Zr^{4+}, which leads to relative strong emission peaking at 461 nm and weak emission at 508 nm. From another perspective, though Eu^{2+} can occupies not only K^+ but also Zr^{4+} sites, the emission spectra still shift to red with the increasing Eu^{2+} content and XRD peaks still shift to big angle which are shown in Figure 9 and Figure 6 left image, and interplanar spacing (d) observed in the HRTEM image (Figure 1a) still turn to small. Because the majority Eu^{2+} that occupying larger K^+ sites will effect interplanar spacing (d) more significant than that minority Eu^{2+} occupying smaller Zr^{4+}.

To further understand the origin of the observed emission center (430-550 nm) in the KZS host, the well-known empirical Van Uitert equation was considered to analyze qualitatively the experimental results. For Eu^{2+} in suitable matrices, the following eq 2 provides a good fit to the emission peak and excitation edge data [35].

$$E = Q[1 - (\frac{V}{4})^{\frac{1}{V}} 10^{-\frac{near}{80}}] \quad (2)$$

In the above eqn (2), E represents the position of the d-band edge in energy for rare earth ions (cm1), Q is the position in energy for the lower d-band edge for the free ions (34 000 cm^{-1} for Eu^{2+}), V is the valency of the activator (Eu^{2+}) (V = 2), n is the number of anions in the immediate shell about the Eu^{2+}, r is the radius of the host cation replaced by the Eu^{2+} ion (in Å), and "ea" is the electron affinity of the atoms that form anions (in eV), which is different when Eu^{2+} is introduced into different anion complexes. Here, ea is approximately determined as 2.5. According to calculation, calculated emission wavelengths of Eu^{2+} ions occupying K^+ cation is 465 nm while Eu^{2+} ions occupying Zr^{4+} cation is 512 nm ,which are close to Gaussian components fitted of PL spectra. It is revealed that Eu^{2+} occupies both K^+ and Zr^{4+} sites and emits blue and green light, respectively.

3.5 Thermal Stability of KZS: 1%Eu^{2+}

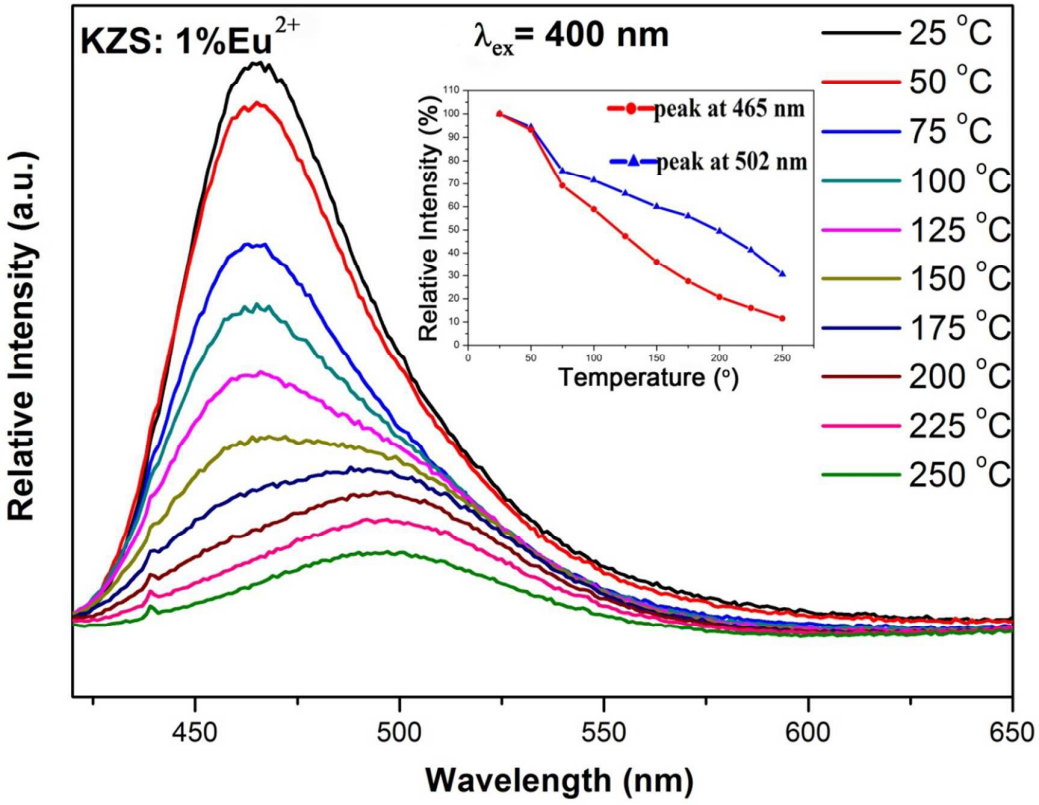

Figure 11 Temperature dependence of KZS: 1%Eu^{2+} PL properties; Inset: Quenching rate contradistinction of two peaks at 465 and 502 nm.

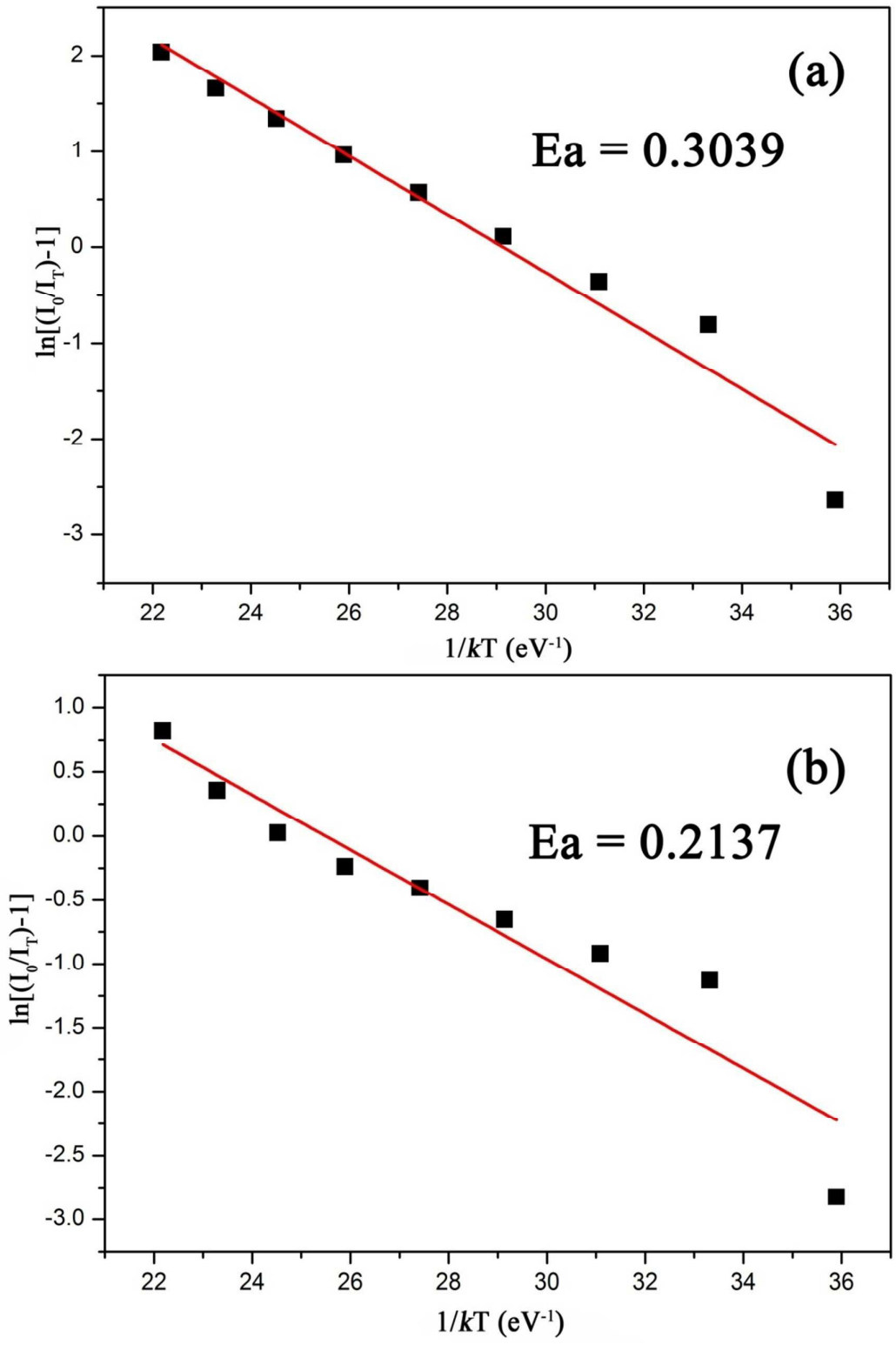

Figure 12 The Arrhenius fitting of the emission intensity of KZS: 1%Eu^{2+}phosphor and the calculated Ea for thermal quenching at different emission sites; (a) peaking at 465 nm; (b) peaking at 502 nm

The temperature dependence of KZS: 1%Eu^{2+} emission spectra upon 400 nm excitation are shown in Figure 11. It can be clearly seen that with temperature increasing, the emission intensity decreases gradually and the emission band goes from one broad peak (peaking at 465 nm) to two broad bands, then to one broad peak (peaking at 502 nm) definitely. Generally, the thermal quenching of emission intensity can be explained by a configurational coordinate diagram in which, through phonon interaction, the excited luminescence center is thermally activated through the crossing point between the excited state and the ground state. This non-radiative transition probability by thermal activation is strongly dependent on temperature resulting in the decrease of emission intensity. At lower Eu^{2+} concentrations (x = 1%), the emission band of Eu^{2+} is mainly dominated by the transition of 5*d* to 4*f* (namely, intrinsic emission). The decrement of emission intensity with the increase of temperature can be ascribed to the temperature-dependent electron–phonon interaction. With the increase of temperature, the electron–phonon interaction increases, which further makes the electrons at the bottom of the 5*d* excited state and shift to the junction of the excited and ground states and then relax to the 4*f* ground state in a nonradiative way. Besides, the different of these two peaks' temperature dependence properties are shown in the Figure 9 inset. At 150 ^{o}C, the emission intensity of the first peak (465 nm) can be kept only 35%, while the second peak (peaking at 502) can be kept 65%. To further verify the difference of temperature-dependent emission intensity (I_T), the activation energy (Ea) was calculated using the Arrhenius equation [36]

$$I_T = \frac{I_0}{1+c\exp(-\frac{\Delta E}{kT})} \quad (3)$$

where I_0 is the initial PL intensity of the phosphor at room temperature, I_T is the PL intensity at different temperatures, c is a constant, ΔE is the activation energy, and k is the Boltzmann constant (8.62×10^{-5} eV). Making this function to do logarithmic transformation can get

$$\ln\left(\frac{I_0}{I_T} - 1\right) = c(-\frac{\Delta E}{kT}) \quad (4)$$

According to the equation, the activation energy ΔE can be calculated by plotting $\ln[(I_0/I_T)-1]$ against $1/kT$, where a straight slope equals ΔE. As shown in Figure 12 (a) and (b), ΔE was found to be 0.3039 eV for first peak (peaking at 465 nm) and 0.2137 eV for second peak (peaking at 502 nm). The discrimination of these two peaks of their temperature dependence properties and Ea can be as assistant proofs of two sites occupying of Eu^{2+}, which have been discussed in 3.4.

3.6 PL decay curves and TRPL Emission of KZS: x%Eu^{2+}

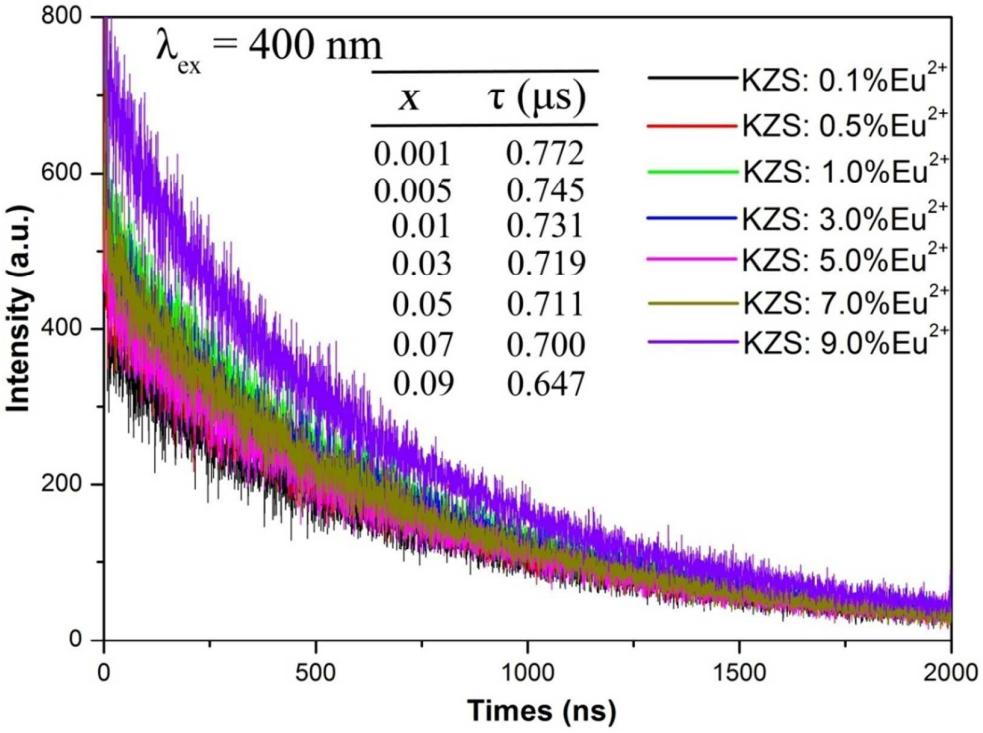

Figure 13 Decay curves of KZS: $x$$Eu^{2+}$ phosphors with different Eu^{2+} contents

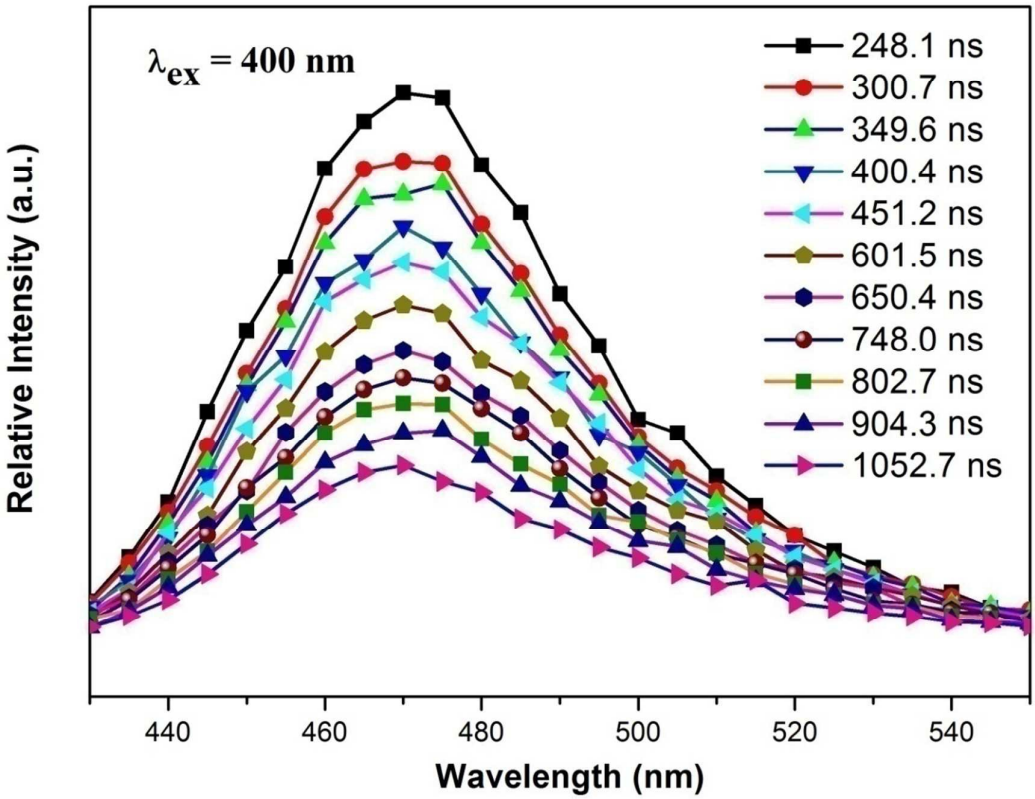

Figure 14 Time-resolved photoluminescence (TRPL) emission spectra of KZS: 1%Eu^{2+}.

Figure 13 presents the room temperature decay curves of the Eu^{2+} luminescence in KZS: $x$$Eu^{2+}$ with different Eu^{2+} contents ($0.001 \leq x \leq 0.09$) upon excitation at 400 nm. The entire decay curve can be well fitted to a second-order exponential decay model because of two occupying sites (K^+ and Zr^{4+}) by the following equation [37]:

$$I(t) = A_1 \exp(-t/\tau_1) + A_2 (-t/\tau_2) \quad (5)$$

Where I is the luminescence intensity; A_1 and A_2 are constants; t is time; and τ_1 and τ_2 are the lifetimes for the exponential components. Further, the average lifetime constant (τ^*) can be calculated as:

$$\tau^* = (A_1\tau_1^2 + A_2\tau_2^2)/(A_1\tau_1 + A_2\tau_2) \quad (6)$$

The calculated average lifetimes of the Eu^{2+} of KZS: 1%Eu^{2+} (x = 0.001, 0.005, 0.01, 0.03, 0.05, 0.07, 0.09) are 772, 745, 731, 719, 711, 700 and 647 ns, respectively. As we know, the lifetime for Eu^{2+} ion is about nanosecond (ns); the relatively shorter lifetime is due to the allowed electric-dipole 5*d*–4*f* transition caused by the poor spatial overlap between the 5*d* and 4*f* orbital. The decay times are in accordance with the most frequent value of the normal Eu^{2+} emission in solids. The lifetime decreases monotonically with the increase of the Eu^{2+} content, indicating an efficient energy transfer among Eu^{2+}.

A series of lifetime decay curves were recorded by monitoring the KZS: 1%Eu^{2+} sample at different wavelengths from 430 to 550 nm at 5 nm intervals. The TRPL spectra shown in Figure 14 were obtained by slicing them. Obviously, the TRPL spectra are clearly constituted by two emission peaks centered at 461 and 508 nm, which has not been found from the emission spectra shown in Fig. 9. Simultaneously, with the time interval prolonging, it was interesting to observe that the ratio of intensity of 461 nm to 508 nm descended significantly, confirming that there are

two light luminescent centers. The occurrence of the two emission peaks further demonstrates Eu^{2+} occupying the two different cationic lattice sites: K^{+} and Zr^{4+} sites.

3.7 PLE and PL Properties of Charge Compensation Phosphors

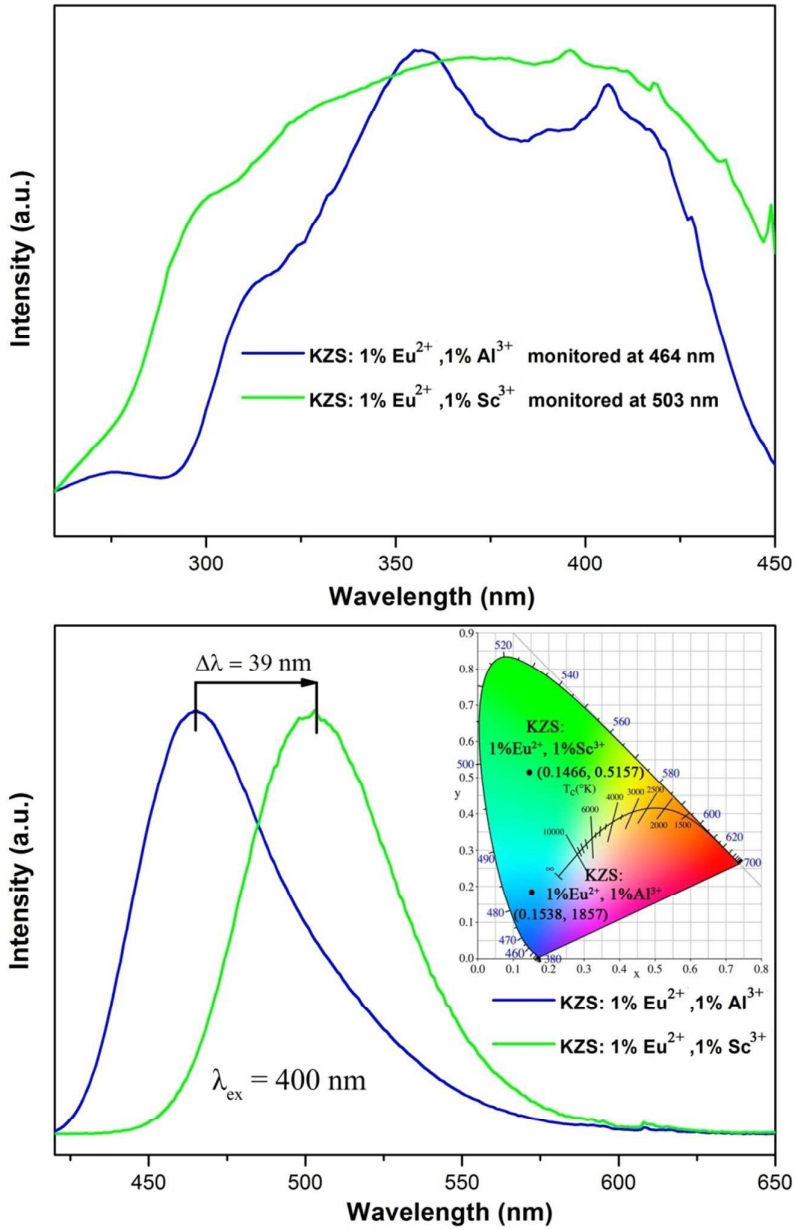

Figure 15 PLE and PL spectra of charge compensation phosphors, Blue line: KZS: 1%Eu^{2+} charge compensation with 1% Al^{3+}; Green line: KZS: 1% Eu^{2+} charge compensation with 1% Sc^{3+}; Inset: CIE chromaticity diagram and coordinate of two charge compensation phosphors

In order to further study luminescence properties of KZS: $x$$Eu^{2+}$, charge compensation samples with different cations are synthesized successfully. The PLE and PL spectra properties are shown in Figure 15. It can be seen that using Eu^{2+}-Al^{3+} as the charge compensation cations pair, the PLE spectrum consists of four peaks or bands which can be attribute to 5d-4F transition of Eu^{2+} ,and the PL spectrum is a broad band at the range of 450-500 nm peaking at 465 nm and emit blue light. The shape and peaks position of PLE and PL spectra are similar with no-charge compensation samples immensely which are pictorial in Figure 8 and 9. However, using Eu^{2+}-Sc^{3+} as the charge compensation cations pair obtains completely different results, which the PLE spectra become broader than Eu^{2+}-Al^{3+} phosphor and the peaks or broads become obscure. Furthermore, the

emission spectra shift to red region about 39 nm under 400 nm excitation and takes on green emission. The calculation Commission International de l' Eclairage (CIE) chromaticity coordinates of Eu^{2+}-Al^{3+} and Eu^{2+}-Sc^{3+} phosphors are shown in the inset of Figure 14 which can provide more intuitive results. The calculated full-width at half-maximum (FWHM) of Eu^{2+}-Al^{3+} emission spectrum is 57 nm and 56 nm for Eu^{2+}-Sc^{3+} emission spectrum.

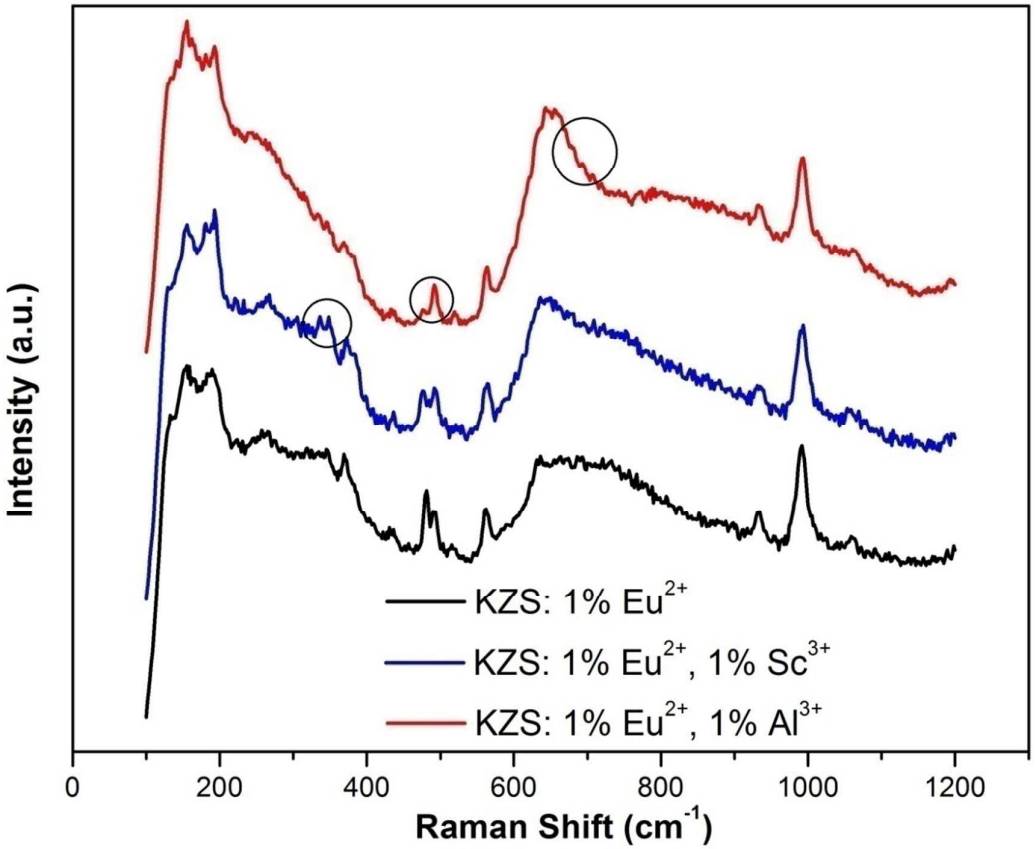

Figure16 The measured Raman spectra of KZS: 1%Eu^{2+} and two charge compensation phosphors

In order to comprehend the different occupying sites of different charge compensation cations pair, Raman spectra of KZS: 1%Eu^{2+} and two charge compensation phosphors are also tested. It can be clearly seen that the Raman spectra of Eu^{2+}-Al^{3+} sample was different at about 500 and 700cm^{-1} compared with no-charge compensation phosphors, that is to say Si-O1 and Si-O2 bonds changed. For the Eu^{2+}-Sc^{3+} sample, Raman spectra at about 320 cm^{-1} is different compared with KZS: 1%Eu^{2+} sample, which is attributed to Zr-O bond [38].

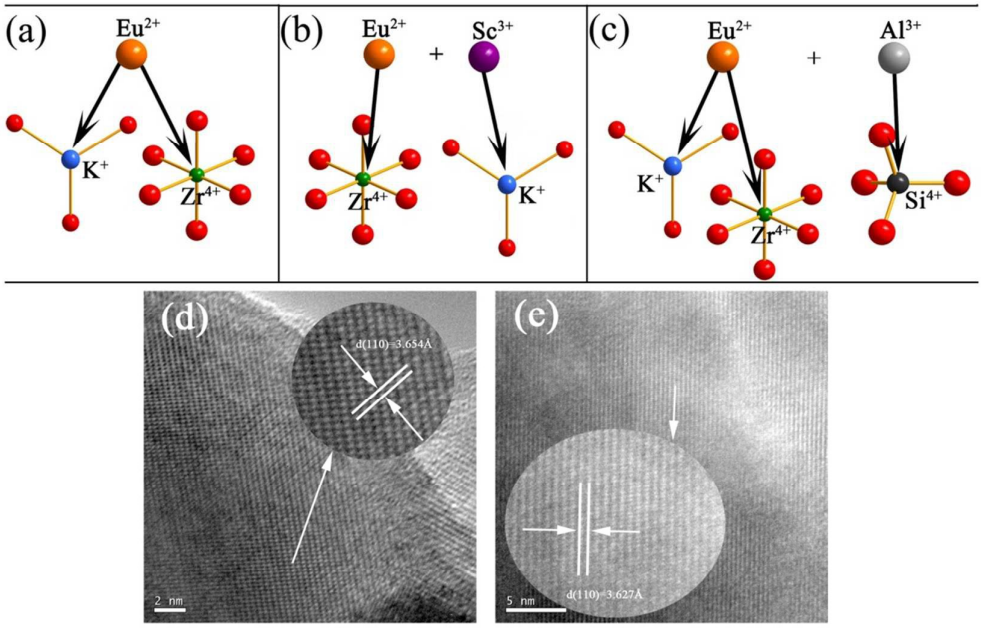

Figure 17 Charge compensation mechanism schematic diagram (a) Eu^{2+} single-doped KZS, (b) Eu^{2+}-Sc^{3+} co-doped KZS, (c) Eu^{2+}-Al^{3+} co-doped KZS; HRTEM image of (d) Eu^{2+}-Al^{3+} charge compensation sample, (e) Eu^{2+}-Sc^{3+} charge compensation sample

According to the discussion and analysis above, possible occupying situation using different dopants are shown in Figure 17. (1) For the Eu^{2+} single-doped, Eu^{2+} can occupy both K^+ and Zr^{4+} sites. The majority of Eu^{2+} substitute K^+ while the minority substitutes Zr^{4+}, which leads to relative strong blue emission and weak green emission. Furthermore, single doped Eu^{2+} also effects XRD peaks positions and interplanar spacing (d) that have been discussed in part of the front. In the situation of Eu^{2+} single-doped KZS, each Eu^{2+} substituting K^+ will produce a positive electricity defect $Eu_K^{\cdot}$. In the same time it will create one vacancy V_K' defect with one negative charge to keep charge balance ($Eu_K^{\cdot} + V_K' \rightarrow (Eu_K V_K)^{\times}$). (2) For Eu^{2+}-Al^{3+} co-doped charge compensation pair, Al^{3+} (0.53 Å) occupies Si^{4+} (0.40 Å) site for their similar ionic radius. The introduction of Al^{3+} does not change the occupying situation of Eu^{2+}. Eu^{2+} still substitutes both K^+ and Zr^{4+} sites and emit blue light consisting of two emission peaks. On the other hand, the measured values of interplanar spacing d(110) is 3.654 Å , larger than no-doped KZS host (3.4680 Å) which is shown in Figure 17(d). That is because larger Al^{3+} occupies smaller Si^{4+}. In the situation of Eu^{2+}-Al^{3+} co-doped KZS, each Eu^{2+} substituting K^+ will produce a positive electricity defect $Eu_K^{\cdot}$. In the same time, each Al^{3+} substituting Si^{4+} will produce a negative electricity defect Al_{Si}' to keep charge balance ($Eu_K^{\cdot} + Al_{Si}' \rightarrow (Eu_K Al_{Si})^{\times}$). (3) For Eu^{2+}-Sc^{3+} co-doped charge compensation pair, If Sc^{3+} occupies K^+ and Eu^{2+} occupies Zr^{4+} it can keep the crystal structure stable. Form charge balance aspect, each Eu^{2+} substituting Zr^{4+} will produce two negative electricity defects Eu_{Si}'' and each Sc^{3+} substituting K^+ will produce two negative electricity defects $Sc_K^{\cdot}$ to keep charge balance ($Eu_{Zr}'' + Sc_K^{\cdot} \rightarrow (Eu_{Zrk} Sc_K)^{\times}$). On the other hand, this situation can avoid crystal structure unstable. Sc^{3+} (0.885 Å) is smaller than K^+ (1.37 Å) and this substitution will lead to shrinking of crystal structure. In the same time, Eu^{2+} is larger than Zr^{4+} and this substitution will lead to expansion of crystal structure. The shrinking and expansion

can be offset. Additional, the discrepancy of Sc^{3+}/K^{+} is $\frac{01.37-0.86}{1.37}\times 100\% = 35\%$ and the discrepancy of Eu^{2+}/Zr^{4+} is $\frac{1.17-0.86}{1.17}\times 100\% = 26.5\%$. They do not have great difference. This situation also provides a proof of Eu^{2+} occupying Zr^{4+} and emit green light just like 3.4 PL properties analysis. Furthermore, the measured values of interplanar spacing d(110) is 3.627 Å , larger than no-doped KZS host (3.4680 Å) which is shown in Figure 17(e). That is because larger Eu^{2+} occupies smaller Zr^{4+}.

4. Conclusions

In summary, a series of novel blue emission $K_2ZrSi_3O_9$: xEu^{2+} phosphors under NUV excitation are synthesized successfully by traditional high temperature solid-state reaction. The critical quenching concentration of Eu^{2+} was about 1 mol%. The CIE chromaticity coordinates and FWHM are (0.1538, 0.1857) and 57 nm. The structure of $K_2ZrSi_3O_9$ was hexagonal (space group *P*63/*m*). It has only one K^{+} site in crystal structure, however $K_2ZrSi_3O_9$: xEu^{2+} shows abnormal asymmetric emission bands peaking at 461 and 508 nm. The reason of this abnormal emission is that Eu^{2+} may not only occupy K^{+} but also Zr^{4+} sites. The temperature dependence of KZS: 1%Eu^{2+} PL properties take on different decay rates of these two emission center. By different charge compensation, $K_2ZrSi_3O_9$: 1%Eu^{2+} possesses different photoluminescence characteristic. $K_2ZrSi_3O_9$: 1%Eu^{2+}, 1%Sc^{3+} emits green light upon 400 nm excitation and the CIE chromaticity coordinates and FWHM are (0.1466, 0.5157) and 56 nm. Blue and green emission can be generated in $K_2ZrSi_3O_9$: Eu^{2+} compound by different charge compensation mechanism. It reveals that $K_2ZrSi_3O_9$: Eu^{2+} possesses remarkable optical properties and can be potential used in NUV-LEDs.

Acknowledgment

This work was supported by the National Natural Science Funds of China (Grant No. 51372105) and the Fundamental Research Funds for the Central Universities (No. lzujbky-2014-231).

Reference

[1] J. M. Phillips, M. E. Coltrin, M. H. Crawford, A. J. Fischer, M. R. Krames, R. M. Mach, G. O. Mueller, Y. Ohno, L. E. S. Rohwer, J. A. Simmons, J. Y. Tsao, *Laser & Photon. Rev. 1*, 2007, **4**, 307

[2] A. Kitai, "Luminescent Materialsand Applications", John Wiley & Sons, Ltd ISBN: 978-0-470-05818-3 (2008)

[3] S. Ye, F. Xiao, Y. X. Pan, Y. Y. Ma, Q. Y. Zhang, *Mater. Sci. Eng. R*, 2010, **71,** 1.

[4] P. F. Smet, A. B. Parmentier, D. Poelman, *J. Electrochem. Soc.*, 2011, **158 (6),** R37.

[5] V. Bachmann, C. Ronda and A. Meijerink, Chem. Mater., 2009, **21,** 2077.

[6] K. Takahashi, N. Hirosaki, R. J. Xie, M. Harada, K. Yoshimura, Y. Tomomura, *Appl. Phys. Lett.*, 2007, **91**, 091923.

[7] C. C. Lin, R. S. Liu, *J. Phys. Chem. Lett.*, 2011, **2,** 1268

[8]. Y. F. Liu, X. Zhang, Z. D. Hao, X.J. Wang, J. H. Zhang, *Chem. Commun.*, 2011, **47**, 10677.

[9]. Y. F, Liu, X. Zhang, Z. D. Hao, X. J. Wang, J. H. Zhang, *J. Mater. Chem*., 2012, **22**, 15146.

[10]. J. K. Li, J.G. Li, S.H. Liu, X. D. Li, X. D. Sun, O. Sakkab, *J. Mater. Chem. C*. 2013, **1**, 7614

[11] C. H. Huang, T. M. Chen, *Inorg. Chem*. 2011, **50**, 5725.

[12] Y. F. Liu, X. Zhang, Z. D. Hao, X. J. Wang, J. H. Zhang, *Chem. Commun.* 2011, **47**, 10677.

[13] W. Lu, N. Guo, Y. C. Jia, Q. Zhao, W. Z. Lv, M. M. Jiao, B. Q. Shao, H. P. You, *Inorg.*

Chem. 2013, **52**, 3007.
[14] D. G. Deng, H. Yu, Y.Q. Li, Y. J. Hua, G. H. Jia, S. L. Zhao, H. P. Wang, L. H. Huang, Y. Y. Li, C. X. Li, S. Q. Xu, *J. Mater. Chem. C*, 2013 **1**, 3194.
[15] K. Y. Jung, H. W. Lee and H. K. Jung, *Chem. Mater.*, 2006, **18**, 2249.
[16] K. Kimoto, R. J. Xie, Y. Matsui, K. Ishizuka, N. Hirosaki, *Appl. Phys. Lett.* 2009**, 94**, 041908
[17] J. Botterman, K. V. Eeckhout, A. J. J. Bos, P. Dorenbos, P. F. Smet, *Opt. Mater. Exp.* 2012, **2**, 341.
[18] Y. Shimomura, T. Honma, M. Shigeiwa, T. Akai, K. Okamoto, N. Kijima, *J. Elect. Soc.* 2007,**154**, 35.
[19] M. A. Lim, J. K. Park, C. H. Kim, H. D. Park, *J. Mater. Sci. Lett.* 2003, 22, 1351.
[20] K. Geng, Z. G. Xia, M. S. Molokeev, *Dalton Trans.*, 2014, **43**, 14092.
[21] J. Y. Zhang , Z. T. Zhang , Z. L. Tang , Y. Tao, X. Long, *Chem. Mater.*, 2002, **14 (7)**, 3005.
[22] W. B. Im, N. George, J. Kurzman, S. Brinkley, A. Mikhailovsky, J. Hu, B. F. Chmelka, S. P. DenBaars, R. Seshadri, *Adv. Mater*. 2011, **23**, 2300.
[23] Z. G. Xia, Y. Y. Zhang, M. S. Molokeev, V. V. Atuchin, Y. Luo, "Linear structural evolution induced tunable photoluminescence in clinopyroxene solid-solution phosphors", *Sci. Rep.* Doi:10.1038/srep03310
[24] M. M. Shang, C. X. Li, J. Lin, *Chem. Soc. Rev.*, 2014, **43 (5)**, 1372.
[25] K. Li, M. M. Shang, D. L. Geng, H. Z. Lian, Y. Zhang, J. Fan, J. Lin, *Inorg. Chem.*, 2014, **53 (13)**, 6743.
[26] M. M. Shang, G. G. Li, D. L. Geng, D. M. Yang, X. J. Kang, Y. Zhang, H. Z. Lian, J. Lin, *J. Phys. Chem. C*, 2012, **116(18)**, 10222.
[27] M. L. Balmer, Y. L. Su, H. W. Xu, E. Bitten, D. McCready, A. Navrotsky, *J. Am. Ceram. Soc.*, 2001, **84 (1),** 153.
[28] D. E. Henshawt, *Mineral. Mag*, 1955, **30,** 585.
[29] A. Orlando, Y. Thibault, A. D. Edgar, *Contrib. Mineral. Petrol.*, 2000, **139**, 136.
[30] W. Zeng, Y. H. Wang, S. C Han, W. B. Chen, G. Li, Y. Z. Wang, Y. Wen, *J. Mater. Chem. C*, 2013, **1**, 3004.
[31] G. Zhu, Y. R. Shi, M. Mikami, Y. Shimomura and Y. H. Wang, *CrystEngComm*, 2014, **16**, 6089.
[32] Y. Sato, H. Kato, M. Kobayashi, T. Masaki, D. H. Yoon, M. Kakinada, *Angew. Chem. Int. Ed.* 2014, **53**, 7756.
[33] J. F. Sun, Z. P. Lian, G. Q. Shen, D. Z. Shen, *RSC Adv.* 2013, **3**, 18395.
[34] R. D. Shannon, *Acta Cryst.*, 1976, **A32**, 751.
[35] C. Y. Liu, Z. G. Xia, Z. P, Lian, J. Zhou, Q. F. Yan, *J. Mater. Chem. C*, 2013, **1**, 7139.
[36] W. Z. Lv, Y. C. Jia, Q. Zhao, W. Lu, M. M. Jiao, B. q. Shao, H. P. You, *J. Phys. Chem. C*, 2014, **118**, 4649.
[37] S. P. Lee, C. H. Huang, T. S. Chan, T. M. Chen, *Appl. Mater. Interfaces.* 2014, **6 (10)**, 7260.
[38] D. A. McKeown, A. C. Nobles, *Phys. Rev.* 1996, **B 54**, 291308

Novel blue and green phosphors yielded in $K_2ZrSi_3O_9$: Eu^{2+} compound by co-doped Al^{3+}, Sc^{3+} for LEDs under NUV excitation